

Complete fusion of ${}^6\text{Li}$ with ${}^{28}\text{Si}$ and ${}^{64}\text{Ni}$ nuclei in the framework of the continuum discretized coupled channel method

S.R. Souza,^{1,2,*} L.F. Canto,¹ and R. Donangelo^{1,3}

¹*Instituto de Física, Universidade Federal do Rio de Janeiro Cidade Universitária,
Caixa Postal 68528, 21941-972 Rio de Janeiro-RJ, Brazil*

²*Departamento de Física, ICEx, Universidade Federal Fluminense,
R. Desembargador Ellis Hermydio Figueira, Atarrado, 27213-145 Volta Redonda - RJ, Brazil*

³*Instituto de Física, Facultad de Ingeniería, Universidad de la República,
Julio Herrera y Reissig 565, 11.300 Montevideo, Uruguay*

(Dated: December 21, 2023)

The complete fusion of ${}^6\text{Li}$ with ${}^{28}\text{Si}$ and ${}^{64}\text{Ni}$ nuclei, ranging from subbarrier energies up to values well above the Coulomb barrier, is studied using the continuum discretized coupled channels method. We investigate the sensitivity of the results to the largest energy used in the discretization of the continuum, including closed channels. Our results reveal that, as long as the states in the continuum are not limited to too small energies, the specific upper bound adopted is not relevant as the complete fusion cross-section is fairly insensitive to it above a threshold. Convergence with respect to this parameter is rapidly reached, so that closed channels play a role only at low collision energies. A good agreement with the available experimental data is obtained.

I. INTRODUCTION

Collisions involving weakly bound projectiles constitute an important tool for studying the effects of their dissociation on different reaction mechanisms [1–3]. Such nuclei may be excited to unbound states during the collision so that the scenario of two [1–6] or three [3, 7–11] fragments interacting with the target must be considered.

The low binding energy of the projectile affects fusion reactions in two ways. First, it leads to a reduction of the Coulomb barrier, arising from the long tail of the projectile's density. This is a static effect that enhances fusion at all collision energies. On the other hand, the low breakup threshold has a strong influence on the reaction dynamics, giving rise to new reaction channels. One possible outcome is the dissociation of the projectile without the absorption of any of the fragments by the target [1, 3, 6, 12–14]. Alternatively, the partial fusion of the projectile, *i.e.*, the absorption of some, but not all of the fragments, leads to the so called incomplete fusion (ICF). There are different ICF processes, characterized by the particular fragment that is captured by the target. There is also the process where all the breakup fragments fuse with the target, which is called sequential complete fusion (SCF). Another possible scenario is the direct complete fusion (DCF), in which the entire projectile fuses with the target without previously dissociating. Although these mechanisms may be treated within the framework of theoretical approaches [1, 2], the SCF cannot be distinguished experimentally from the DCF as both lead to the same compound nucleus, and their sum is named complete fusion (CF). The excitation of these unbound states reduces DCF, which is usually the

leading fusion mechanism. This leads to a suppression of CF at all collision energies. Then, the net effect of the low binding energy on the CF cross section is the result of these competing effects. Comparisons of theoretical and experimental CF cross sections with predictions of barrier penetration models that disregard the cluster structure of the projectile indicate suppression above the Coulomb barrier and enhancement at sub-barrier energies [1–3].

Different theoretical approaches have been developed to study the fusion processes taking place in collisions of weakly bound projectiles (see the review articles [1–3], and references therein). The most realistic ones are based on the Continuum Discretized Coupled Channel method (CDCC), to deal with coupled channel equations involving the continuum [7, 10, 11, 15–21]. Presently, a few computer codes to implement this method are available [4, 22, 23]. However, the CDCC alone does not give individual cross sections for the CF or ICF processes. For this purpose, complementary assumptions must be made. It is also worth mentioning the indirect determination of the CF cross section for the ${}^{6,7}\text{Li} + {}^{209}\text{Bi}$ systems [24], which was extracted from the total reaction cross section, by subtracting its inelastic, elastic breakup, and inclusive nonelastic breakup components.

The first CDCC based calculations of CF and ICF cross sections were made by Hagino *et al.* [25] and by Diaz-Torres and Thompson [26], for the ${}^{11}\text{Be} + {}^{208}\text{Pb}$ system. ${}^{11}\text{Be}$ is a weakly bound nucleus, that breaks up into a ${}^{10}\text{Be}$ cluster and one neutron. These works adopted a short-range imaginary potential depending exclusively on the projectile-target distance. Their basic assumption was that absorption in the bound channels contributed to CF, whereas absorption in unbound channels corresponded to ICF of the ${}^{10}\text{Be}$ cluster. Since this cluster is much heavier than the neutron, in an

* Corresponding author: srsouza@if.ufrj.br

unbound channel, it must be close to the projectile, while the neutron is far away. Then, it is reasonable to assume that absorption by the imaginary potential corresponds to ICF. However, this approach has important limitations. First, it cannot be used for projectiles like ${}^6,7\text{Li}$, which break up into fragments with comparable masses. Besides, this method cannot determine individual cross section for the two ICF processes which, in principle, could be determined experimentally.

For the calculation of individual ICF cross sections, the imaginary potential must be a sum of terms, each one accounting for the absorption of a fragment of the projectile. Diaz-Torres, Thompson and Beck [27], and Descouvemont *et al.* [7] performed CDCC calculations using an imaginary potential of this kind. However, they only evaluated the TF cross section, which was identified with the total absorption of the imaginary potential.

Recently, Rangel *et al.* [28] developed a CDCC based method to evaluate the CF and ICF cross sections, henceforth referred to as the CF-ICF model. Their CDCC calculations were similar to those of Ref. [27], but they made additional assumptions to relate the observable cross sections to quantities that could be obtained from the CDCC calculations. This method was applied to collisions of several weakly bound projectiles on heavy targets [28–31]. In the CF-ICF model, the CF and ICF cross sections are expressed in terms of radial integrals of the imaginary potentials. These integrals, require scattering wave functions in bound and unbound channels, evaluated with great accuracy in the internal region of the Coulomb barrier. In Refs. [28–31], the wave functions were obtained by FRESKO, which discretize the continuum by the *bin method* [4]. This code is optimized to give accurate elastic and breakup cross sections. These cross sections are expressed in terms of the S-matrix, which is extracted from the asymptotic forms of the wave functions. Thus, it is not particularly concerned with wave functions in the inner region of the barrier. For this reason, the convergence of the CF and ICF cross sections of Refs. [28–31] demanded great care, mainly at energies well below the Coulomb barrier.

In the present work, we discuss a new implementation of the CF-ICF model, where the CDCC equations are solved by the R-matrix formalism of Ref. [32], and the CF and ICF cross sections are calculated by the expressions in the appendix of Ref. [29]. Then, we evaluate the CF cross section for collisions of ${}^6\text{Li}$ with targets lighter than the ones studied in previous applications of the CF-ICF model. The remainder of this manuscript is organized as follows. The main features of the CDCC treatment are reviewed in Sect. II, whereas the main results are presented in Sect. III. A brief summary of our main findings is made in Sect. IV.

II. THEORETICAL FRAMEWORK

We consider the collision of a projectile that dissociates into two fragments, c_1 and c_2 . In the case of ${}^6\text{Li}$, c_1 is the deuteron and c_2 is the alpha particle. The real part of the projectile-target interaction has the form,

$$V(\vec{R}, \vec{r}) = V_1(r_1) + V_2(r_2), \quad (1)$$

where r_i is the distance between c_i and the target, and $V_i(r_i)$ is the corresponding potential. Throughout the present work, these interactions are given by the Akyüz-Winther potential [33, 34]. The vectors \vec{r}_1 and \vec{r}_2 are related to the vector between the projectile and the target, \vec{R} , and the vector joining the two fragments, \vec{r} , by the relations

$$\vec{r}_1 = \vec{R} + \frac{2}{3} \vec{r}, \quad \vec{r}_2 = \vec{R} - \frac{1}{3} \vec{r}.$$

For the imaginary part of the potential, we follow Ref. [29], adopting different forms for the bound and unbound channels. The details can be found in Ref. [29].

In the CDCC method [1, 4], the scattering wavefunction $\Psi^{(+)}(\vec{k}_0, \vec{R})$ describing the colliding nuclei, whose incident relative momentum is $\hbar\vec{k}_0$, is expanded on eigenstates $|\varphi_{\alpha,i}\rangle$ of the intrinsic projectile's hamiltonian and scattering states $\psi_{\alpha,i}^{(+)}(\vec{k}_0, \vec{R})$, projected on channel $\{\alpha, i\}$:

$$\Psi^{(+)}(\vec{k}_0, \vec{R}) = \sum_{\alpha,i} \psi_{\alpha,i}^{(+)}(\vec{k}_0, \vec{R}) |\varphi_{\alpha,i}\rangle, \quad (2)$$

where α denotes the set of quantum numbers associated with the channel and i represents the index of an energy in the set of the discrete values used for each α . From this expansion, one may write the set of equations which couple the different channels considered in the calculation [32], with the same total angular momentum J and parity π :

$$\left[-\frac{\hbar^2}{2\mu} \left(\frac{d^2}{dR^2} - \frac{L(L+1)}{R^2} \right) + (\varepsilon_i^{jl} - \varepsilon_0) - E_{\text{CM}} \right] \phi_{\alpha,i}^{J\pi}(R) = \sum_{\alpha',i'} V_{\alpha i, \alpha' i'}^{J\pi}(R) \phi_{\alpha',i'}^{J\pi}(R). \quad (3)$$

Above, μ represents the reduced mass of the projectile and target nuclei, L denotes the quantum number associated with their relative orbital angular momentum, and $\phi_{\alpha,i}^{J\pi}(R)$ symbolizes the radial component of $\psi_{\alpha,i}^{(+)}(\vec{k}_0, \vec{R})$. The center of mass kinetic energy of the colliding partners and the projectile's intrinsic energy in the entrance channel are respectively denoted by E_{CM} and ε_0 . The i -th eigenvalue of the intrinsic projectile's hamiltonian, associated with a relative orbital (l) and total (j) angular momenta quantum numbers, is represented by ε_i^{jl} . After

TABLE I. Barriers of the $V_{PT}(R)$ and $V_{00}(R)$ potentials (in MeV), for the systems studied in this work.

System	V_{PT}^B	V_{00}^B
${}^6\text{Li} + {}^{28}\text{Si}$	7.0	6.4
${}^6\text{Li} + {}^{64}\text{Ni}$	12.4	11.6

performing the angular integrations over the projectile-target and fragment-core coordinates on the multipole expansion of the potential acting between the target and the clusters, the coupling between the different channels $V_{\alpha i, \alpha' i'}^{J\pi}(R)$, is given by [6]:

$$V_{\alpha i, \alpha' i'}^{J\pi}(R) = (-1)^{J-s} i^{l'+L'-l-L} \hat{j} \hat{j}' \hat{l} \hat{l}' \hat{L} \hat{L}' \\ \times \sum_{\lambda} (-1)^{\lambda} \begin{pmatrix} l & l' & \lambda \\ 0 & 0 & 0 \end{pmatrix} \begin{pmatrix} L & L' & \lambda \\ 0 & 0 & 0 \end{pmatrix} \left\{ \begin{matrix} j & L & J \\ L' & j' & \lambda \end{matrix} \right\} \\ \times \left\{ \begin{matrix} j & l & s \\ l' & j' & \lambda \end{matrix} \right\} \int_0^{\infty} dr \tilde{\varphi}_i^{jl}(r) V_{\lambda}(r, R) \tilde{\varphi}_{i'}^{j'l'}(r). \quad (4)$$

In this expression, $V_{\lambda}(r, R)$ corresponds to the coefficient of the multipole expansion [29] and $\tilde{\varphi}_i^{jl}(r)$ is the radial part of the projectile internal wavefunction. The quantum numbers l, j , and L are associated with the index $\alpha = \{l, j, L\}$. The spin of the projectile's fragment is denoted by s and we consider spinless cores. In the present case, $s = 1$, as we focus on the dissociation of the ${}^6\text{Li}$ into a deuteron and a ground state ${}^4\text{He}$ nucleus. We adopt the usual notation $\hat{x} = \sqrt{2x+1}$, besides the representation $()$ and $\{\}$ for the Wigner 3J and 6J symbols, respectively.

In collisions of ${}^6\text{Li}$ with tightly bound targets, which will be considered in the present work, the off-diagonal matrix elements of Eq. (4) couple the elastic channel (the only bound channel of the system) to the continuum. On the other hand, the diagonal matrix element of the potential,

$$V_{00}(R) = (\varphi_0 | V_1 + V_2 | \varphi_0), \quad (5)$$

where φ_0 stands for the ground state of ${}^6\text{Li}$, plays the role of the real part of the optical potential in the elastic channel. The barrier of this potential is denoted by V_{00}^B .

It is interesting to compare V_{00}^B to the barrier of the ${}^6\text{Li}$ -target AW potential when the cluster structure of the projectile is neglected. This potential and its Coulomb barrier are denoted by $V_{PT}(R)$ and V_{PT}^B , respectively. Table I shows the barriers of the two potentials, for the systems studied in the present work. One concludes that the reductions for the ${}^6\text{Li} + {}^{28}\text{Si}$ and ${}^6\text{Li} + {}^{64}\text{Ni}$ systems are of 0.6 and 0.8 MeV, respectively.

A. Intrinsic projectile states

To obtain the intrinsic projectile states, we follow Refs. [6, 35] and expand $\tilde{\varphi}_i^{jl}(r)$ on a Lagrange-Laguerre basis:

$$\tilde{\varphi}_i^{jl}(r) = \frac{1}{h^{1/2}} \sum_{k=1}^N c_k^{jl} f_k(r/h), \quad (6)$$

where

$$f_k(x) = (-1)^j x_k^{1/2} \left(\frac{x}{x_k} \right) \frac{L_N(x)}{x-x_k} \exp[-x/2], \quad (7)$$

$L_N(x)$ is the Laguerre polynomial of order N , x_k its k -th root and h is a scaling parameter. One should note that the use of this basis leads to square integrable wavefunctions due to the exponential factor. To obtain the bound and continuum internal pseudo states of the projectile, the expansion given by Eq. (6) is inserted into the eigenvalue equation associated with the internal projectile hamiltonian. This leads to [35]:

$$\sum_{k'=1}^N [T_{k,k'}^l + v_{jl}(x_k h) \delta_{kk'}] c_{k'}^{jl} = c_k^{jl} \varepsilon_i^{jl}, \quad (8)$$

where $\delta_{kk'}$ corresponds to the Kronecker delta function, $T_{k,k'}^l$ denotes the matrix elements of the kinetic energy operator acting on the relative coordinates of the projectile fragments, and $v_{jl}(x_k h)$ is the total potential between them at separation $r = x_k h$. Explicit expressions for $T_{k,k'}^l$ may be found in Ref. [35]. The solution of this system of equations leads to the eigenvalues $\{\varepsilon_1^{jl}, \dots, \varepsilon_N^{jl}\}$ and the eigenvectors $\{(c_1^{jl,1}, c_2^{jl,1}, \dots, c_N^{jl,1}), \dots, (c_1^{jl,N}, c_2^{jl,N}, \dots, c_N^{jl,N})\}$. The latter are needed to build $\tilde{\varphi}_i^{jl}(r)$ through Eq. (6). Therefore, the number of states considered in the calculation depends on N and h , which are parameters of the calculation. However, the final results must be stable for relative small variations on specific choices of these parameters.

The potential energy above is split into two terms. The Coulomb one reads:

$$v_{\text{Coul}}(r) = \begin{cases} \frac{Z_{c_1} Z_{c_2} e^2}{r}, & r \geq R_C \\ \frac{Z_{c_1} Z_{c_2} e^2}{2R_C} \left[3 - \frac{r^2}{R_C^2} \right], & r \leq R_C, \end{cases} \quad (9)$$

where $R_C = r_{0C}(A_{c_1}^{1/3} + A_{c_2}^{1/3})$ and $r_{0C} = 1.3$ fm. Above, c_i represents the i -th cluster and A_{c_i} (Z_{c_i}) is its mass (atomic) number. As in Ref. [36], the nuclear interaction between the clusters is approximated by:

$$v_{\text{nuc}}(r) = -V_0 F(r) + A_{SO} \left(\frac{\hbar}{m_{\pi} c} \right)^2 \frac{1}{r} \frac{dF(r)}{dr} \vec{l} \cdot \vec{s}, \quad (10)$$

and

$$F(r) = \frac{1}{1 + \exp[(r - R_0)/a]}, \quad (11)$$

where m_π is the pion mass. Since in this work we consider the ${}^6\text{Li}$ projectile, we adopt the following parameters for the nuclear interaction between the clusters [30]: $R_0 = r_0(A_{c1}^{1/3} + A_{c2}^{1/3})$, $r_0 = 1.0046$ fm, and $a = 0.7$ fm in all cases. We employ $V_0 = 78.38$ MeV and $A_{SO} = 0$ for $j = 1$ and $l = 0$, otherwise $V_0 = 80.0$ MeV and $A_{SO} = 2.5$ MeV. This choice allows one to reproduce the experimental dissociation energy (1.47 MeV) of the ${}^6\text{Li}$ into the deuteron and the ground state ${}^4\text{He}$ nucleus, with $J^\pi = 1^+$ ($l = 0$), as well as its resonances [27, 30]. The energy of the pseudo states obtained with these parameters, using $N = 35$ and $h = 0.5$, are exhibited in Fig. 1 for selected values of j and l . The results show that the density of states is much smaller at energies above 5 MeV than below it. Therefore, one should expect important contributions to the continuum-continuum coupling from such low lying energy states.

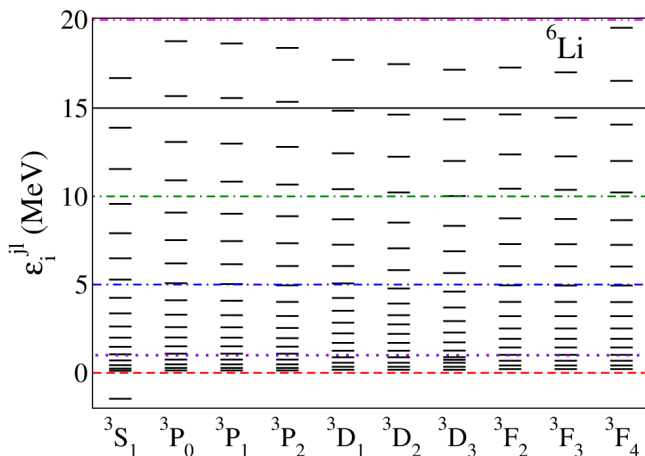


FIG. 1. (Color online) Energy levels of pseudo states, for different j and l , describing the two cluster states of ${}^6\text{Li}$ nucleus for $N = 35$ and $h = 0.5$. For details, see the text.

B. Channel wavefunctions and the fusion cross-section

To solve Eqs. (3), the potentials needed to calculate the multipole coefficients $V_\lambda(r, R)$ must be specified. Besides the Coulomb one, whose parameterization is similar to that given by Eq. (9), one adopts, as in Ref. [36], the Akyüz-Winther potential (AW) [33, 34] for the nuclear interactions between the fragments and the target.

Different techniques have been employed to solve the system of coupled equations (3) [4, 5, 14, 32, 37–39].

Owing to the robustness of its numerical solutions, we follow Refs. [6, 23, 32] where the application of the R-matrix theory to this problem is carefully described. A difficulty of this treatment is that, for each value of J^π and L , it requires the inversion of a large matrix, whose size depends on the number of the radial mesh points adopted in the calculations, multiplied by the number of channels included. For a fine discretization of the radial mesh and a large number of channels, very large matrices are rapidly obtained and their inversion may be prohibitively time consuming. To mitigate this difficulty, the space is divided into \mathcal{N}_s spherical shells delimited by $a_{k-1} \leq R \leq a_k$, $1 \leq k \leq \mathcal{N}_s$, $a_0 = 0$, $a_{\mathcal{N}_s} = R_{\max}$. The latter denotes the largest radial distance on the mesh. Within the k -th shell, N_k points are used in the discretization. In this way, one needs to invert \mathcal{N}_s matrices of much smaller sizes, which considerably speeds up the numerical implementation. As is detailed described in Ref. [23], $\phi_{\alpha,i}^{J^\pi}(R)$ is expanded on a Gauss-Lagrange basis within each shell:

$$\phi_{\alpha,i}^{J^\pi}(R) = \sum_{n=1}^{N_k} c_n^{J^\pi \alpha, i}(k) g_n^{(k)}(R), \quad a_{k-1} \leq R \leq a_k. \quad (12)$$

In the above expression, the base function $g_n^{(k)}(R)$ is:

$$g_n^{(k)}(R) = (-1)^{N_k+k} \sqrt{\Delta_k x_n^{(k)} (1 - x_n^{(k)})} \times \left(\frac{R}{a_{k+1} x_n^{(k)}} \right)^{\delta_{k,1}} \frac{P_{N_k} \left(\frac{2R - a_k - a_{k-1}}{\Delta_k} \right)}{R - \Delta_k x_n^{(k)} - a_k}, \quad (13)$$

where $\Delta_k = a_k - a_{k-1}$, $P_{N_k}(x)$ is the Legendre polynomial of order N_k , and $x_n^{(k)}$ is the n -th root of $P_{N_k}(2x_n^{(k)} - 1) = 0$. This basis leads to efficient evaluation of the matrix elements [32] entering the calculations of the multipole expansion $V_\lambda(r, R)$ [29].

The numerical implementation of the R-matrix method with Lagrange meshes is carefully described in Refs. [23, 32]. Since our implementation follows these references, we do not furnish further details. One should note that the quantities \mathcal{N}_s , $\{a_1, \dots, a_{\mathcal{N}_s}\}$, $\{N_1, \dots, N_{\mathcal{N}_s}\}$, and R_{\max} are parameters of the calculations, whose influence on the final results must be checked in actual applications.

For the calculation of the CF cross section, we use the version of the CF-ICF model presented in Ref. [30]. The cross section is evaluated in three steps.

1. Using the expressions in the appendix of Ref. [29], we evaluate the DCF probability for each angular momentum, P_J^{DCF} . We also evaluate individual fusion probabilities for each fragment, denoted by $P_J^{(1)}$ and $P_J^{(2)}$. Note that $P_J^{(1)}$ and $P_J^{(2)}$ are inclusive probabilities. That is, the probability of fusion of one of the fragments, whatever happens to the other.

2. Then, using the above results, we obtain the observable CF probability, P_J^{CF} , by adopting the intuitive assumption of Ref. [30],

$$P_J^{SCF} = P_J^{(1)} P_J^{(2)}, \quad (14)$$

and thus

$$P_J^{CF} = P_J^{DCF} + P_J^{(1)} P_J^{(2)}.$$

3. Finally, the CF cross section is obtained by carrying out the angular momentum sum

$$\sigma_{CF} = \frac{\pi}{k_0^2} \sum_J (2J+1) P_J^{CF}. \quad (15)$$

We emphasize that we adopt the prescription of Ref. [29] for the imaginary potential. For bound channels, it depends exclusively on the projectile-target distance, and is denoted by $W_{PT}(R)$. For unbound channels, it is a sum of two terms, each one representing the absorption of one of the fragments by the target. It is denoted by $W_1(r_1) + W_2(r_2)$. The details of these potentials can be found in Ref. [29].

Finally, as in Ref. [30], we introduce the spectroscopic amplitude α in the coupling between bound and unbound states of the ${}^6\text{Li}$ clusters, in order to take into account the fact that the $d + {}^4\text{He}$ cluster structure is an approximation to the actual ground state of the nucleus. We adopt the same value $\alpha = 0.7$ used in that study.

III. RESULTS

Before discussing the main results of the present investigation, we report the tests made on their sensitivity to the parameters of the calculations. For simplicity, we use shells such that $a_{k+1} - a_k = 5.0$ fm and $N_k = 20$, $1 \leq k \leq \mathcal{N}_s$, but different spacing and number of points may be adopted for each one. We have found that finer discretizations do not affect the results presented in this work. Our tests also suggest that $R_{\max} = 150$ fm ($\mathcal{N}_s = 30$) is sufficient for the results presented below.

Since the coupling with states in the continuum plays a relevant role in the fusion process involving weakly bound nuclei [2, 14, 17, 27, 29, 30], the inclusion of such states must be carefully considered. Therefore, we examined the sensitivity of our results to the discretization of the continuum using different values of (j, l) . For both systems considered in the present study, we find that, at energies below the Coulomb barrier, varying the largest value of l (l_{\max}) from 3 to 4 changes the CF cross-section approximately 10%. The differences decrease very rapidly as the collision energy increases, being negligible at a few MeV above the barrier. Thus, the use of $l_{\max} = 3$ is a good compromise between computational efficiency and precision. One should note that, if energies

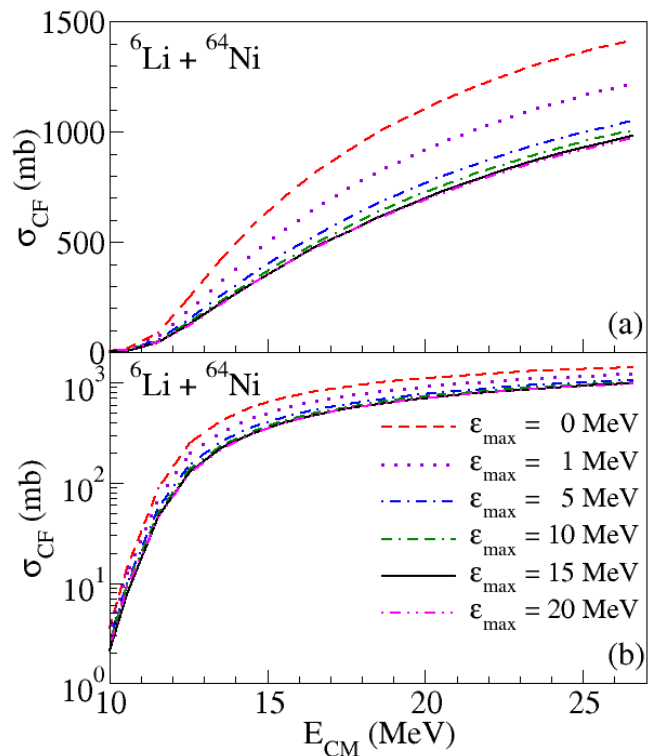


FIG. 2. (Color online) Complete fusion cross-section for different values of ε_{\max} , for collisions between the ${}^6\text{Li}$ and the ${}^{64}\text{Ni}$ nuclei at different values of the center of mass energy. Panel (a) displays the results in linear scale whereas the semi-log scale is used in panel (b). For details, see the text.

in the continuum up to $\varepsilon_{\max} = 20$ MeV are allowed, this leads to a system of more than 600 coupled equations for $l_{\max} = 4$. There are, in this way, \mathcal{N}_s complex matrices of size $600N_k \times 600N_k$ to be inverted for each (J^π, L) .

To investigate the influence of ε_{\max} on the fusion cross-section, we show, in Fig. 2, the CF cross-sections for the ${}^6\text{Li} + {}^{64}\text{Ni}$ system as a function of E_{CM} obtained using different values of ε_{\max} . We consider collision energies ranging from 10 to 27 MeV. The lowest energy corresponds to ~ 2 MeV below the Coulomb barrier of the folded potential, $V_{00}(R)$, given in Table I. The results reveal that the CF cross sections is fairly sensitive to this parameter. This is because the coupling with states in the continuum redistributes flux among the channels, removing contributions from the bound to the unbound ones. The latter leads to the incomplete fusion of one of the fragments [30], at the cost of lowering the DCF and, consequently, the CF if the contribution due to SCF does not tip the balance in favor of CF. This is the case for the systems studied in this work. Nevertheless, the differences between the results for $\varepsilon_{\max} = 10$ and $\varepsilon_{\max} = 20$ MeV are typically of the order of 5%, throughout the energy interval of the calculations. Convergence is practically reached for $10 \text{ MeV} \leq \varepsilon_{\max} \leq 20 \text{ MeV}$. Our findings are in agreement with those of Refs. [27, 30] that obtained

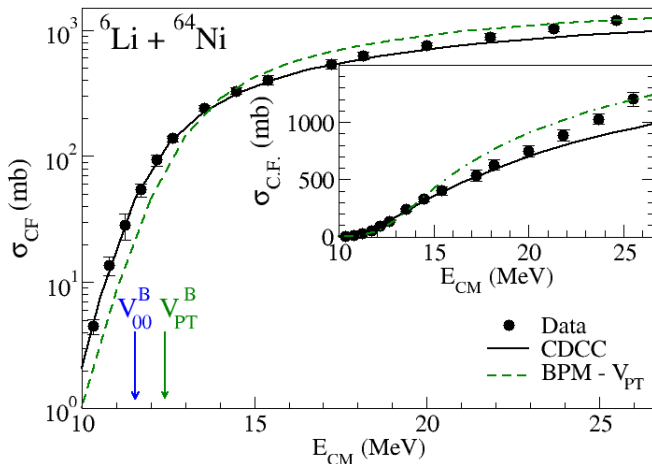


FIG. 3. (Color online) Complete Fusion cross-section as a function of the center of mass energy of the colliding nuclei. The data are from Ref. [42]. For details, see the text.

converged results using similar upper bounds. The fact that the largest changes occur for $\varepsilon_{\max} \leq 5$ MeV, even for $E_{\text{CM}} \gg 5$ MeV, does not mean that closed channels do not play a relevant role in the coupling among the channels. Indeed, we have checked that, for $\varepsilon_{\max} = 15$ MeV, the CF cross-section at $V_{00}^B - 2$ MeV changes by about 20% if all closed channels are excluded from the calculation. They correspond to approximately 24% of the total number of channels. Note that setting $\varepsilon_{\max} = 0$ is equivalent to switching off all couplings with the continuum. Then, the set of coupled equations reduces to a single equation for the elastic channel, with the potential $V_{00}(R)$. In this way, the dashed line in Fig. 2 is the cross section of a one-channel calculation with this potential, which is virtually the same as the cross section of the barrier penetration model (BPM) for the same potential [40]. This cross section contains the static effects of the barrier lowering, resulting from the low breakup threshold of ${}^6\text{Li}$. Thus, comparing it to the CF cross section one finds that the latter is suppressed at all collision energies. This is a consequence of the breakup couplings on complete fusion.

Contrary to the conclusions of Ref. [41], our results suggest that closed channels affect the fusion cross-section only at low collision energies as convergence with respect to ε_{\max} is reached at relatively small values, compared with those obtained in that work. By contrast, our results reveal that the coupling with low lying states in the continuum are more relevant in this context since the CF cross-section is very sensitive to states with energy $\varepsilon_{\max} \lesssim 5$ MeV. Therefore, as long as one is interested in the fusion process, we find that there is no need to include very high energy continuum states in CDCC calculations.

We now compare, in Fig. 3, the CF cross section of our calculations to the experimental data reported in Ref. [42]. The full line depicts our CDCC results using

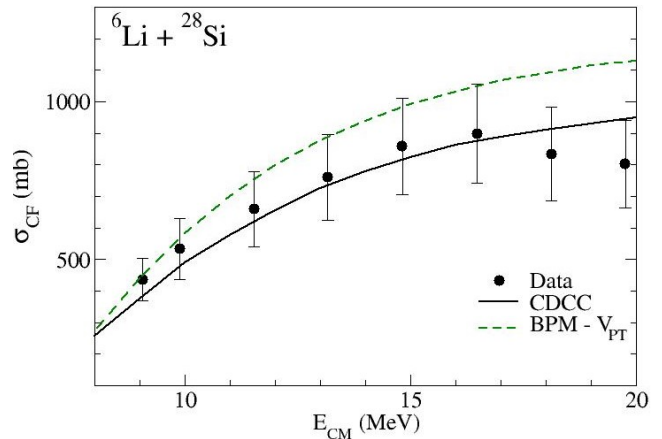


FIG. 4. (Color online) Same as Fig. 3 for the ${}^6\text{Li} + {}^{28}\text{Si}$ Nuclei. The data are from Ref. [43, 44]. For details, see the text.

$\varepsilon_{\max} = 15$ MeV, which is adopted in all the calculations below. The agreement with the experimental results is very good, with significant deviations observed only at the highest energies. To assess the net effect of the low binding energy of ${}^6\text{Li}$ on CF, we also show the BPM cross section for the potential $V_{PT}(R)$ (green dashed-line). Since this potential neglects the cluster structure of the projectile, its BPM cross section does not contain the barrier lowering effect. Then comparing the BPM and the CF cross sections, one assesses the net effect of the low binding energy of the projectile. As observed for other weakly bound systems [1–3], one finds enhancement at sub-barrier energies and suppression above the Coulomb barrier. At the highest energies considered in Fig. 3, one finds a suppression factor of 0.77.

In order to check the validity of the above conclusions to collisions involving lighter targets, we have also carried out similar CDCC calculations for the ${}^6\text{Li} + {}^{28}\text{Si}$ system. Our findings concerning the convergence of the calculated cross-sections also hold in this case. Figure 4 exhibits a comparison of the CF cross section of our CDCC calculations to the CF data of Refs. [43, 44]. The data and the calculations are for collision energies between 8 and 20 MeV, which are higher than the Coulomb barriers V_{00}^B and V_{PT}^B for the ${}^6\text{Li} + {}^{28}\text{Si}$ system (see Table I). The agreement between theory and experiment is very good, except at the highest collision energies, where the CDCC calculations overpredict the data. The figure also shows the cross section of the BPM with the potential $V_{PT}(R)$ (green dashed line). Comparing it to the CF cross sections we find that the latter is enhanced at sub-barrier energies and suppressed above the barrier, as in the collision with the ${}^{64}\text{Ni}$ target. In this case, the suppression factors at the highest energies is 0.84, which is slightly larger than for the heavier ${}^{64}\text{Ni}$ target. This indicates that the

suppression for the lighter target is weaker.

Thus, our CDCC calculations give a fairly accurate description of the experimental CF cross-sections employing states in the continuum with energy up to 15 MeV.

IV. CONCLUDING REMARKS

We have studied the CF cross sections in collisions of ${}^6\text{Li}$ projectiles with ${}^{64}\text{Ni}$ and ${}^{28}\text{Si}$ targets. For this purpose, we performed CDCC calculations using the pseudo states approach, and evaluated the CF cross sections using the CF-ICF model. We have investigated the influence of the largest energy ε_{max} allowed in the continuum states in CDCC calculations on the complete fusion cross-sections. Collisions of ${}^6\text{Li}$ projectiles with medium (${}^{64}\text{Ni}$) and light (${}^{28}\text{Si}$) targets have been considered. In both cases, we found that the complete fusion is very sensitive to ε_{max} in the range $0 \leq \varepsilon_{\text{max}} \lesssim 5$ MeV. Convergence is virtually reached between 10 MeV to 15 MeV, so that values around 10 MeV lead to a fairly good approximation to the converged results as the deviations are on the order of 5%. Nevertheless, closed channels must be in-

cluded in the calculations at low collision energies as their removal leads typically to 20% deviations in the cases we examined. The good agreement of the theoretical calculations with the available experimental data for the two systems studied gives support to the robustness of our conclusions.

ACKNOWLEDGMENTS

This work was supported in part by the Brazilian agencies Conselho Nacional de Desenvolvimento Científico e Tecnológico (CNPq), the Uruguayan agencies Programa de Desarrollo de las Ciencias Básicas (PEDECIBA) and the Agencia Nacional de Investigación e Innovación (ANII) for partial financial support. This work has been done as a part of the project INCT-FNA, Proc. No.464898/2014-5. We also thank the Núcleo Avançado de Computação de Alto Desempenho (NACAD), Instituto Alberto Luiz Coimbra de Pós-Graduação e Pesquisa em Engenharia (COPPE), Universidade Federal do Rio de Janeiro (UFRJ), for the use of the supercomputer Lobo Carneiro and VERSATUS HPC where part of the calculations have been carried out.

-
- [1] L. F. Canto, P. R. S. Gomes, R. Donangelo, J. Lubian, and M. S. Hussein, *Phys. Rep.* **596**, 1 (2015).
 - [2] K. Hagino, K. Ogata, and A. M. Moro, *Prog. Part. Nucl. Phys.* **125**, 103951 (2022).
 - [3] Antonio M. Moro, *Models for nuclear reactions with weakly bound systems* (2018).
 - [4] I. J. Thompson, *Comput. Phys. Rep.* **7**, 167 (1988).
 - [5] M. Yahiro, M. Nakano, Y. Iseri, and M. Kamimura, *Prog. Theo. Phys.* **67**, 1467 (1982).
 - [6] T. Druet, D. Baye, P. Descouvemont, and J.-M. Sparenberg, *Nucl. Phys. A* **845**, 88 (2010).
 - [7] P. Descouvemont, T. Druet, L. F. Canto, and M. S. Hussein, *Phys. Rev. C* **91**, 024606 (2015).
 - [8] P. Descouvemont, T. Druet, L. F. Canto, and M. S. Hussein, in *NUBA Conference Series - 1: Nuclear Physics and Astrophysics*, *Journal of Physics: Conference Series*, Vol. 590 (2015) p. 012008.
 - [9] T. Matsumoto, E. Hiyama, M. Yahiro, K. Ogata, Y. Iseri, and M. Kamimura, *Nucl. Phys. A* **738**, 471 (2004).
 - [10] M. Rodríguez-Gallardo, J. M. Arias, J. Gómez-Camacho, R. C. Johnson, A. M. Moro, I. J. Thompson, and J. A. Tostevin, *Phys. Rev. C* **77**, 064609 (2008).
 - [11] M. Rodríguez-Gallardo, J. M. Arias, J. Gómez-Camacho, A. M. Moro, I. J. Thompson, and J. A. Tostevin, *Phys. Rev. C* **80**, 051601 (2009).
 - [12] J. A. Tostevin, F. M. Nunes, and I. J. Thompson, *Phys. Rev.* **C63**, 024617 (2001).
 - [13] P. Chau-Huu Tai, *Eur. Phys. J. A.* **51**, 166 (2015).
 - [14] W. Chen, H. Guo, T. Ye, Y. Ying, W. Sun, and Y. Han, *J. Phys. G: Nucl. Part. Phys.* **49**, 075104 (2022).
 - [15] Y. Sakuragi, M. Yahiro, and M. Kamimura, *Prog. Theor. Phys.* **70**, 1047 (1983).
 - [16] Y. Sakuragi, M. Yahiro, and M. Kamimura, *Prog. Theor. Phys. Suppl.* **89**, 136 (1986).
 - [17] N. Austern, Y. Iseri, M. Kamimura, M. Kawai, G. Rauscher, and M. Yahiro, *Phys. Rep.* **154**, 125 (1987).
 - [18] I. J. Thompson and F. M. Nunes, *Nuclear Reactions for Astrophysics: Principles, Calculation and Applications*, 1st ed. (Cambridge University Press, 2009).
 - [19] T. Matsumoto, E. Hiyama, K. Ogata, Y. Iseri, M. Kamimura, S. Chiba, and M. Yahiro, *Phys. Rev. C* **70**, 061601 (2004).
 - [20] M. Yahiro, Y. Iseri, H. Kameyama, M. Kamimura, and M. Kawai, *Prog. of Theor. Phys. Suppl.* **89**, 32 (1986).
 - [21] M. Gómez-Ramos and A. M. Moro, *Phys. Rev. C* **95**, 034609 (2017).
 - [22] K. Hagino, N. Rowley, and A. T. Kruppa, *Comp. Phys. Commun.* **123**, 143 (1999).
 - [23] P. Descouvemont, *Phys. Rev. C* **93**, 034616 (2016).
 - [24] J. Lei and A. M. Moro, *Phys. Rev. Lett.* **122**, 042503 (2019).
 - [25] K. Hagino, A. Vitturi, C. H. Dasso, and S. M. Lenzi, *Phys. Rev. C* **61**, 037602 (2000).
 - [26] A. Diaz-Torres and I. J. Thompson, *Phys. Rev. C* **65**, 024606 (2002).
 - [27] A. Diaz-Torres, I. J. Thompson, and C. Beck, *Phys. Rev. C* **68**, 044607 (2003).
 - [28] J. Rangel, M. Cortes, J. Lubian, and L. F. Canto, *Phys. Lett. B* **803**, 135337 (2020).
 - [29] M. R. Cortes, J. Rangel, J. L. Ferreira, J. Lubian, and L. F. Canto, *Phys. Rev. C* **102**, 064628 (2020).
 - [30] J. Lubian, J. L. Ferreira, J. Rangel, M. R. Cortes, and L. F. Canto, *Phys. Rev. C* **105**, 054601 (2022).
 - [31] J. L. Ferreira, J. Rangel, J. Lubian, and L. F. Canto, *Phys. Rev. C* **107**, 034603 (2023).
 - [32] P. Descouvemont and D. Baye, *Rep. Prog. Phys.* **73**,

- 036301 (2010).
- [33] R. A. Broglia and A. Winther, *Heavy Ion Reactions* (Westview Press, Cambridge, MA, 2004).
- [34] O. Akyüz and A. Winther, in *Nuclear Structure of Heavy Ion Reaction*, edited by R. A. Broglia, C. H. Dasso, and R. A. Ricci (North Holland, 1981) proc. E. Fermi Summer School of Physics.
- [35] D. Baye, *physica status solidi (b)* **243**, 1095 (2006).
- [36] G. D. Kolinger, L. F. Canto, R. Donangelo, and S. R. Souza, *Phys. Rev. C* **98**, 044604 (2018).
- [37] K. Alder, F. Roesel, and R. Morf, *Nucl. Phys. A* **284**, 145 (1977).
- [38] T. Matsumoto, T. Kamizato, K. Ogata, Y. Iseri, E. Hiyama, M. Kamimura, and M. Yahiro, *Phys. Rev. C* **68**, 064607 (2003).
- [39] M. Rhoades-Brown, M. H. Macfarlane, and S. C. Pieper, *Phys. Rev. C* **21**, 2436 (1980).
- [40] L. F. Canto, R. Donangelo, M. S. Hussein, P. Lotti, J. Lubian, and J. Rangel, *Phys. Rev. C* **98**, 044617 (2018).
- [41] W. Chen, D. Y. Pang, H. Guo, Y. Tao, W. Sun, and Y. Ying, *Phys. Rev. C* **107**, 064610 (2023).
- [42] Md. Moin Shaikh, Subinit Roy, S. Rajbanshi, M. K. Pradhan, A. Mukherjee, P. Basu, S. Pal, V. Nanal, R. G. Pillay, and A. Shrivastava, *Phys. Rev. C* **90**, 024615 (2014).
- [43] Mandira. Sinha and J. Luian, *Eur. Phys. J. A.* **53**, 224 (2017).
- [44] M. Sinha, H. Majumdar, P. Basu, S. Roy, R. Bhattacharya, M. Biswas, M. K. Pradhan, R. Palit, I. Mazumdar, and S. Kailas, *Eur. Phys. J. A* **44**, 403 (2010).